의학박사 학위논문

인간 유방암세포주 이종이식 종양모델 마우스의 확산강조 MR 영상 텍스쳐 분석을 이용한 종양이질성 연구

2014 년 8 월

서울대학교 대학원

의학과 영상의학전공

윤 보 라

의학박사 학위논문

인간 유방암세포주 이종이식 종양모델 마우스의 확산강조 MR 영상 텍스쳐 분석을 이용한 종양이질성 연구

2014 년 8 월

서울대학교 대학원

의학과 영상의학전공

윤 보 라

Doctoral Thesis

Intratumoral Heterogeneity of Breast Cancer Xenograft Models: Texture Analysis of Diffusion-Weighted MR Imaging

August 2014

The Graduate School, Seoul National University

College of Medicine, Radiology

Bo La Yun

인간 유방암세포주 이종이식 종양모델 마우스의 확산강조 MR 영상 텍스쳐 분석을 이용한 종양이질성 연구

지도교수 조 나 리 야

이 논문을 의학과 박사 학위논문으로 제출함
2014 년 4 월

서울대학교 대학원
의학과 영상의학전공
윤 보 라

윤보라의 박사학위논문을 인준함
2014 년 6 월

위 원 장 _____ (인)

부 위 원 장 _____ (인)

위 원 _____ (인)

위 원 _____ (인)

위 원 _____ (인)

ABSTRACT

Intratumoral Heterogeneity of Breast Cancer Xenograft Models: Texture Analysis of Diffusion-Weighted MR Imaging

Bo La Yun

College of Medicine, Radiology

The Graduate School

Seoul National University

Objectives: To investigate whether there is an association between texture analysis parameters of the apparent diffusion coefficient (ADC) maps and histopathologic features of MCF-7 and MDA-MB-231 xenograft models.

Materials and Methods: With approval of the animal care committee, MCF-7 estradiol (+), MCF-7 estradiol (-), and MDA-MB-231 xenograft models were made using SCID mice. Diffusion-weighted MR images were obtained on a 9.4T system. First order texture analysis and second order texture analysis using grey level co-occurrence matrix (GLCM) of ADC maps were performed. Image parameters and

histopathologic features were compared among the MCF-7 estradiol (+), MCF-7 estradiol (-), and MDA-MB-231 groups using the analysis of variance test. Intraobserver agreement of the texture parameters was also evaluated. The relationship between image parameters and histopathologic features, including the proportion and pattern of necrosis, mean and difference of Ki-67, and microvessel density (MVD), were analyzed using Pearson correlation analysis. The results were based on 12 tumors in the MCF-7 estradiol (+) group, 9 tumors in the MCF-7 estradiol (-) group, and 6 tumors in the MDA-MB-231 group.

Results: In the first order texture analysis, the MCF-7 estradiol (+) group showed higher standard deviation, maximum value, skewness, and kurtosis of the ADC maps than either the MCF-7 estradiol (-) group or the MDA-MB-231 group ($P < 0.01$ for all). In the second order texture analysis, the contrast of the MCF-7 estradiol (+) and (-) groups were higher than that of the MDA-MB-231 group ($P = 0.004$). The correlation of the texture analysis (COR) of MDA-MB-231 group was higher than that of the MCF-7 estradiol (+) or (-) groups ($P < 0.001$). The ICCs between two repeated measurements of texture parameters were more than 0.85 in all parameters, which means good agreement, except in minimum value. Histopathologic feature analysis showed that the $Ki\text{-}67_{mean}$ and $Ki\text{-}67_{diff}$ of the MCF-7 estradiol (+) group were higher than that of the MCF-7 estradiol (-) or MDA-MB-231 groups ($P < 0.05$). The MVD_{mean} and MVD_{diff} of the MDA-MB-231 group were higher than those of the MCF-7 groups ($P < 0.001$). Diffuse multifocal necrosis was more frequently found ($P < 0.001$) in the MDA-MB-231 group than in MCF-7 groups. The standard deviation ($r = 0.622$, $r = 0.437$), skewness ($r = 0.404$, $r = 0.484$), and kurtosis ($r = 0.408$, $r = 0.452$) of the ADC maps were correlated with $Ki\text{-}67_{mean}$ and $Ki\text{-}67_{diff}$ ($P < 0.05$ for all).

The COR (r = -0.388, P = 0.045) of the ADC maps were inversely correlated with Ki-67$_{diff}$ (P = 0.045). The skewness (r = -0.643, r =-0.464), kurtosis (r = -0.581, r = -0.389) and contrast (r = -0.473, r = -0.549) of ADC maps were inversely correlated with MVD$_{mean}$ and MVD$_{diff}$ (P < 0.05 for all). The COR of ADC maps was correlated with MVD$_{mean}$ and MVD$_{diff}$ (r = 0.588, P = 0.001; r = 0.580, P = 0.002). Contrast was inversely correlated with the proportion of necrosis (r = -0.438, P = 0.022).

Conclusions: Texture analysis of ADC maps may determine the intratumoral spatial heterogeneity of necrosis patterns, amount of cellular proliferation, and vascularity in MCF-7 and MDA-MB-231 xenograft models.

Key words: Animal; Breast Neoplasms; Diffusion Magnetic Resonance Imaging; Image Interpretation, Computer-Assisted.

Student number: *2012-30515*

CONTENTS

LIST of TABLES

LIST of FIGURES

INTRODUCTION

It has been well established that breast cancer is a heterogeneous disease. Gene expression profiling analysis has resulted in the classification of several breast cancer subtypes (luminal A, luminal B, HER2-positive, and triple-negative), which show various prognosis and therapeutic outcomes (1). Systemic treatment recommendations follow the subtype classification, and current approaches to molecular biomarker testing focus on this inter-patient tumor heterogeneity. However, as predictive biomarkers evolve during tumor progression or treatment, the intratumoral heterogeneity is also believed to be related to clinical outcomes (2). Several ongoing clinical trials are using multiregional sampling to evaluate intratumoral heterogeneity and evolution in relation to drug treatment. However, the genomic assessment of intratumoral heterogeneity for clinical application has many practical challenges, including imprecision in the spatial orientation of tumor sample blocks or sampling bias from data obtained in a limited geographical region. The development of non-invasive imaging techniques to characterize or monitor intratumoral heterogeneity would be ideal.

Diffusion-weighted magnetic resonance imaging (DW-MRI) with apparent diffusion coefficient (ADC) has been increasingly used in the field of oncology. Signals from DW-MRI originate from restrictions to the random movement of water between cell membranes of tissues, which reflects tumor cellularity and the integrity of cell membranes (3). Quick imaging without the need for an exogenous contrast medium allows the clinical application of DW-MRI with ADC to expand from the differentiation of benign and malignant tumors, the screening of cancers, and the

monitoring of the response to chemotherapeutic treatment to prognostic applications (4-9). Recently, a study using the xenograft tumor model found that ADC values of the solid portion of tumors are correlated with intratumoral necrosis and microvessel density in prostate cancers (10). Additionally, distributions of ADC values have correlated with tumor growth rates and the expression of Ki-67, hypoxia inducible factor 1 alpha (HIF-1α), and vascular endothelial growth factor receptor (VEGFR)-2 in breast cancers (11).

Texture analysis, which relies on mathematical methods to describe relationships between the grey level of pixels and their spatial information, has been emerging in the field of medical imaging for the purpose of establishing a quantification technique for spatial heterogeneity (12, 13). Grey level co-occurrence matrix (GLCM) is the one of the most frequently used texture analysis method in the field of medical imaging. GLCM analysis calculates relative frequency matrix generated by counting the occurrences of intensity pairs between the current and neighboring pixels in a given grey-level image (14). So, it has been applied better tissue characterization and prediction of therapy response and survival in contrast-enhanced MRI and ^{18}F-FDG-PET scans through evaluation of inter-relationship of the pixels (15-22). However, few studies have reported its application to in evaluating the intratumoral heterogeneity of various breast cancer xenograft model subtypes, as characterized by DW-MRI.

Thus, the purpose of this study was to determine whether there is a relationship between texture analysis parameters of the ADC maps and histopathologic features of MCF-7 and MDA-MB-231 xenograft models.

MATERIALS AND METHODS

This study was approved by the Institutional Animal Care and Use Committee (IACUC) of the Seoul National University Hospital Biomedical Research Institute and was performed under the guidelines of the National Institutes of Health for the care and use of laboratory animals.

MDA-MB-231 and MCF-7 Tumor Models

MCF-7 and MDA-MB-231 cell lines (American Type Culture Collection, Manassas, VA, USA) were cultured and prepared for inoculation in an orthotropic xenograft model. Twenty-one female nonobese diabetic-severe combined immunodeficient (NOD-SCID) mice, aged six weeks (Orient, Seoul, Korea), received subcutaneous injections of approximately $5x10^6$ cells (in 50 μl serum free media) mixed with 50 μl Matrigel (BD Biosciences, Franklin Lakes, NJ, USA) into bilateral abdominal mammary fat pads. Fourteen mice for MCF-7 groups were pre-treated with 3 mg/kg of beta-estradiol 17-cypionate (Sigma-Aldrich, St. Louis, MO, USA) by subcutaneous injection, starting two weeks before the cell implantation. The pre-treated mice were then divided into two groups; MCF-7 estradiol (+) and MCF-7 estradiol (-). The MCF-7 estradiol (+) group received an additional weekly estradiol injection until the MR imaging. For the MCF-7 estradiol (-) group, additional estradiol supplement was not given after cell implantation. Seven mice were implanted with the MDA-MB- 231 cell line and did not receive estradiol supplement. MR images were acquired when the maximal diameter of the tumor reached 10 mm.

DW-MRI and Texture Analysis

DW-MRI was performed with a 9.4-T MR imaging system (Varian, Magnex

Scientific Ltd., Palo Alto, CA, USA) equipped with a surface coil. The animal was anesthetized with isoflurane (1%–2% in 100% oxygen) during MR imaging. Body temperature and respiratory rate were continuously monitored using pressure-sensitive and rectal temperature probes. An air warmer was used to maintain body temperature throughout the experiments. The MR imaging protocol included the following sequences: (a) a sagittal T2-weighted fast spin-echo sequence (FSE) (repetition time /echo time, 3000 msec /25 msec; matrix, 128 × 96; field of view, 30 × 20 mm; section thickness, 1 mm; gap, 1 mm); (b) axial diffusion-weighted (DW) images obtained by FSE (repetition time /echo time , 3000 msec /27 msec; average, 2; echo train length, 4; matrix, 96 × 128; field of view, 20 × 30 mm; section thickness, 1 mm; gap, 0-0.2 mm) with eight b factors (b = 0, 50, 100, 150, 200, 400, 600 and 800 sec/mm^2) in three orthogonal gradient directions (x, y, and z). Bilateral implanted tumors were imaged together.

Image analysis was performed by an experienced radiologist (B. L.Y., 8 years of experiences in imaging analysis). Tumor volume was calculated in sagittal T2-weighted FSE images and axial DW-FSE (b = 0) images by the equation: volume = 3.14 * height * width * length/6. The ADC, based on the Stejskal and Tanner (23) equation, was calculated using the linear regression algorithm for best fitting the points for b versus ln(SI), where SI is the signal intensity from a region of interest (ROI) of the images acquired at the eight b values. A home-made software package to obtain ADC maps on a pixel-by-pixel basis was developed in IDL platform (ITT Visual Information Solutions, USA). ROIs were drawn along the outline of the tumor in the ADC image showing the largest tumor diameter. For the first order texture analysis, the mean, standard deviation, quartiles, minimum, maximum, skewness, and kurtosis

of the ADC maps were calculated. To evaluate spatial relationship of pixels, the second order texture analysis (GLCM) was used. Among several calculated features derived from GLCM, we used five features related with regional heterogeneity which were frequently used previous studies (12). Contrast, entropy, homogeneity, uniformity, and correlation (COR) of the ADC values within the ROI were calculated using in-house GLCM software as follows (24):

$$\text{Contrast} = \sum_{n=0}^{N-1} n^2 \left\{ \sum_{i=1}^{N} \sum_{j=1}^{N} p(i,j) \right\}, |i-j| = n$$

$$\text{Entropy} = -\sum_{i=0}^{N-1} \sum_{j=0}^{N-1} p\,(i,j)\, log\big(p(i,j)\big)$$

$$\text{Homogeneity} = \sum_{i=0}^{N-1} \sum_{j=0}^{N-1} \frac{p(i,j)}{1+(i-j)^2}$$

$$\text{Uniformity} = \sum_{i=0}^{N-1} \sum_{j=0}^{N-1} \{p(i,j)\}^2$$

$$\text{Correlation (COR)} = \sum_{i=0}^{N-1} \sum_{j=0}^{N-1} \frac{(ij)p(i,j) - \mu_x \mu_y}{\sigma_x \sigma_y}$$

Variables *i* and *j* represent the grey values in the ADC map, $p(i,j)$ is the (i,j)th entry in a normalized GLCM, and N is the number of distinct grey levels in an image. Variables μ_x, μ_y, are means of p_x and p_y, and variables σ_x, σ_y are standard deviations of p_x and p_y.

To evaluate the intraobserver variability, the same radiologist (B. L. Y.) measured the same parameters 4 months later.

Quantification of Histopathologic Features

Immediately after MR image acquisition, all mice were euthanized with CO_2 narcosis followed by a thoracotomy. Tumors were excised with overlying skin. The cephalic direction of the skin was marked. Paraffin-embedded tissues were cut into 5-μm thick sections in the plane parallel to the axial MR image. Two pathologists (S.Y. P. and M. H. J.), who were blinded to tumor cell type, performed all pathologic examinations. Hematoxylin and eosin (H&E) staining was performed for the analysis of the distribution and amount of necrosis. The proportion of necrosis within the tumor was quantified. The distribution of necrosis was classified as a central and diffuse multifocal pattern.

Immunohistochemical staining of the proliferation marker, Ki-67, using a rabbit monoclonal antibody (Abcam, Cambridge, UK; Clone SP6, dilution 1:100) was conducted. The Ki-67 antibody-stained slides were scanned using an AperioScanScope (Aperio Technologies, Vista, CA, USA) with a nuclear algorithm. The areas of highest and lowest density of Ki-67-positive cells were selected. The Ki-67 index was calculated by the fraction of Ki-67 positive cells on samples of at least 500 tumor cells. The mean Ki-67 index for the lowest and highest density area is labeled $Ki\text{-}67_{mean.}$ The difference in the Ki-67 index between the lowest and highest density areas is represented by $Ki\text{-}67_{diff.}$ The pan-endothelial marker, CD34, was stained using a rabbit monoclonal antibody (Abcam, Cambridge, UK; Clone EP373Y, dilution 1:100) for microvessel staining. The lowest and highest vascular areas were selected on low power fields (×40), and microvessel density (MVD) was calculated when CD34-positive endothelial or clustered cells were present under high power field (×200) examination. The mean MVD in the highest and the lowest vascular areas is denoted as MVD_{mean}. The MVD difference between the lowest and highest vascular

areas are denoted as MVD_{diff}.

Exclusions

Of the 21 mice, two mice (including one MCF-7 estradiol (-) and one MDA-MB 231) were excluded due to unwanted death during MR examinations. To minimize the effect of tumor volume on heterogeneity, we only included tumors with a volume in the range of 500- 1500 mm^3, because larger tumors tended to have higher hypoxic fraction and necrosis (25). Finally, 12 tumors of the MCF-7 estradiol (+) group, 9 tumors of the MCF-7 estradiol (-) group, and 6 tumors in the MDA-MB-231 group were included for the final analysis.

Data and Statistical analysis

Statistical analyses were performed using PASW statistics 18 (IBM SPSS, Chicago, IL, USA) and MedCalc 10.0.0.0 (MedCalc Software, Ostend, Belgium). A normal distribution was verified by the Kolmogorov-Smirnov test.

The first and second order texture analysis parameters were compared among the three groups using the analysis of variance (ANOVA) test or the Kruskal-Wallis test. If the results were significant, post-hoc analysis using Bonferroni method was performed. For the comparison of the necrosis patterns, the Fisher's exact test was performed. Then, we performed a correlation analysis between the texture analysis parameters from DW-MRI and histopathologic parameters using the Pearson correlation test. Intraobserver variability of ROI measurement was evaluated by using intraclass correlation coefficients (ICCs) with a two-way mixed consistency model. When the P value was less than 0.05, the results were considered significant.

RESULTS

No difference was found in tumor volumes among the MCF-7 estradiol (+) group, MCF-7 estradiol (-) group, and MDA-MB-231 group (mean ± SD, 808.1 ± 143.9 mm^3, 757.1 ± 142.7mm^3, 944.9 ± 341.7 mm^3, respectively; P=0.221) (Figure 1A).

Texture Parameters

The MCF-7 estradiol (+) group showed a significantly higher standard deviation (398 × 10-6mm2/sec, 235 × 10-6mm2/sec and 213 × 10-6mm2/sec, respectively; P < 0.001), higher maximum value (2610 × $10^{-6}mm^2$/sec, 1904 × $10^{-6}mm^2$/sec, and 2149 × $10^{-6}mm^2$/sec, respectively; P < 0.001), higher skewness (2.66, 1.82, and 1.23, respectively; P < 0.001), and higher kurtosis (7.32, 4.69, and 3.45, respectively; P = 0.001) than the MCF-7 estradiol (-) or MDA-MB-231 groups. Higher standard deviation indicates much dispersion of the distribution of the values from the mean. Higher kurtosis indicates sharp peak and/ or wide tail of the distribution of the values. Higher positive skewness indicates more asymmetric distribution of the values compared to the normal distribution. Our results showed a more heterogeneous intratumoral ADC pixel value in the MCF-7 estradiol (+) group (Table 1 and Figure 1). With regard to the second order texture GLCM analysis, the contrast of the MCF-7 estradiol (+) or estradiol (-) groups was significantly higher than that of the MDA-MB-231 group (476, 536, and 288, respectively; P = 0.004), and the COR of the MCF-7 estradiol (+) group and estradiol (-) group were significantly lower than that of MDA-MB-231 group (0.437 × 10^{-3}, 0.824x10^{-3}, and 2.00x10^{-3}, respectively; P < 0.001; Table 1 and Figure 2). Contrast measures the local variations in signal intensity

between a pixel and a neighbor pixel. COR measures a joint probability occurrence between a pixel and a neighbor pixel in a whole region. Our results showed that MCF-7 groups had more various signal intensities between neighboring pixel pairs than MDA-MB-231 group and had less joint probability occurrences between neighboring pixel pairs.

There was no difference in the mean, median, first and third quintile ADC value, entropy, homogeneity, and uniformity among the three groups on texture analysis. The ICCs between two repeated measurements of texture parameters were more than 0.85 in all parameters but minimum value (Table 2).

Histopathologic Features

The proportion of necrosis in MCF-7 estradiol (+) and (-) groups was lower than that in the MDA-MB-231 group (23.8%, 18.3% and 35.8%, respectively; P = 0.008). Central pattern necrosis was found in both MCF-7 groups but not in the MDA-MB-231 group, whereas diffuse multifocal pattern necrosis was more frequently found in the MDA-MB-231 group ($P < 0.001$).With regard to Ki-67, the MCF-7 estradiol (+) group showed the highest $Ki\text{-}67_{mean}$ value followed by the MDA-MB-231 group and the MCF-7 estradiol (-) group. $Ki\text{-}67_{diff}$ was higher in the MCF-7 estradiol (+) group than in MDA-MB-231 or MCF-7 estradiol (-) groups. The MDA-MB-231 group showed a higher MVD_{mean} and MVD_{diff} than those of the MCF-7 estradiol (+) or estradiol (-) groups (Table 3, Figure 3).

Relationship between Texture and Histopathologic features

The representative cases showed the relationship between histopathologic

findings and ADC maps (Figure 4).The proportion of necrosis was inversely correlated with contrast (r = -0.438, P = 0.022) and was correlated with COR (r = 0.540, P = 0.004). Ki-67_{mean} and Ki-67_{diff} were correlated with the standard deviation (r = 0.622, P = 0.001 and r = 0.437, P = 0.023), skewness (r = 0.404, P = 0.036 and r = 0.484, P = 0.011), and kurtosis (r=0.408, P = 0.035 and r = 0.452, P = 0.018) of the ADC maps. And the COR of the ADC maps was inversely correlated with Ki-67_{diff} (r = -0.388, P=0.045; Figure 5). MVD_{mean} and MVD_{diff} were inversely correlated with the skewness (r = -0.643, P < 0.001 and r = -0.464, P = 0.015), kurtosis (r = -0.581, P = 0.001 and r = -0.389, P = 0.045), contrast (r = -0.473, P = 0.013 and r = -0.549, P = 0.003) of the ADC maps. MVD_{mean} and MVD_{diff} was correlated with COR of ADC maps (r=0.588, P=0.001; r=0.580, P=0.002; Figure 6).

DISCUSSION

In our study, the ADC map of the MCF-7 xenograft model with exogenous estradiol supplementation showed more heterogeneous texture parameters, central necrosis, and higher Ki-67 values, whereas MDA-MB-231 showed less heterogeneous texture parameters, diffuse multifocal necrosis, and higher MVD. The standard deviation, skewness, and kurtosis of the ADC map correlated with Ki-67mean and Ki-67diff, whereas, the COR of the ADC map inversely correlated with Ki-67diff. In addition, skewness, kurtosis, and contrast inversely correlated with MVDmean and MVDdiff, whereas, the COR correlated with MVDmean and MVDdiff.

Our results are consistent with those of a previous study, in which triple negative breast cancer xenograft models showed a correlation between distributions of

the ADC value in DW-MRI and tumor growth rates or the expression of Ki-67, HIF-1α, and VEGFR-2 (11). However, these authors did not investigate differences between the estrogen receptor (ER) (+) and ER (-) subtypes of breast cancer models. In our study, MCF-7 cell lines represent ER (+) breast cancer and MDA-MB-231 cell lines represent the triple negative breast cancer subtype. Compared to the MCF-7 estradiol (-) or MDA-MB 231 tumors, the MCF-7 estradiol (+) tumors showed a higher $Ki\text{-}67_{mean}$, indicating higher cell proliferation. The increased proliferation of ER (+) breast tumors relative to ER (-) MDA-MB-231 tumor scan be explained by the mitogenic effect of estradiol, which has been well established (26, 27). Histogram (first order texture) analysis of the MCF-7 estradiol (+) ADC map showed higher standard deviation, higher skewness (asymmetry of pixel distribution), and higher kurtosis (peakness of pixel distribution) than the MDA-MB-231 ADC map, suggesting wider distribution, higher asymmetry, or a sharper ADC distribution peak, which, in general, indicates a greater heterogeneity of ADC histogram(28, 29). Furthermore, Pearson correlation analysis also revealed a positive correlation between these first order texture parameters and higher $Ki\text{-}67_{mean}$ and $Ki\text{-}67_{diff}$ values.

Second order texture analysis using GLCM is necessary for assessing intratumoral heterogeneity as the grey scale histogram analysis inherently lacks spatial information of parameters reflecting the distribution of cellularity or necrosis (30). Compared to the MCF-7-derived tumors with or without exogenous estradiol supplementation, the MDA-MB-231-derived tumors showed low contrast, high COR in the GLCM analysis, a diffuse multifocal necrosis pattern, and a higher MVDmean at histopathology. Moreover, Pearson correlation analysis showed that MVDmean and MVDdiff inversely correlated with the skewness, kurtosis and contrast of the ADC

values. Additionally, MVDmean and MVDdiff correlated with COR. Therefore, we can infer that a lower contrast, or a lower difference between neighboring pixel values, indicates a lower spatial heterogeneity, which is affected by the vascularity of the tumor. The COR indicates the linearity of the neighboring pixel values. Considering the schematic drawing of Figure 7, even though the three matrices have same mean and standard deviation with two grey levels, the mosaic pattern shows the lowest COR (-0.09), and the largest area of same value pattern shows the highest COR (0.75). The large area of similar pixel values leads to a higher COR; the COR value is 1 when all values in matrix are same. Thus, the higher COR of the MDA-MB-231 compared to the MCF-7 estradiol (+) group or MCF-7 estradiol (-) group can be explained by the diffuse multifocal pattern necrosis found in the MDA-MB-231 group. Higher vascularity (higher MVD) observed in the MDA-MB-231 group may prevent confluent necrosis, leading to preservation of linearity of neighboring pixel values of the ADC map. Based on our results, second texture analysis of ADC maps can provide quantitative spatial information of the necrosis pattern as described by the vascularity.

The use of a 9.4T animal MRI is another notable aspect of our study. Improvement of signal to noise ratio through subcutaneous tumor location and high-field strength is the main factor that enabled our texture analysis for tumor models (31). DW-MRI is an appealing imaging modality to examine tumor aggressiveness and responsiveness to therapy in the field of oncology because it can be easily incorporated into clinical practice due to its non-invasiveness and quick acquisition time without contrast agents (32). Tumors with lower ADC values have been reported to be correlated with higher cellularity, a tortuous extracellular space, and a rapid

tumor growth rate (33, 34). In an animal model, DW-MRI showed higher sensitivity than T2-weighted MR images in detection of colorectal liver metastasis (35). A recent study reported that the ADC values of epithelial-like xenograft tumors were lower than those of mesenchymal-like tumors (36). In clinical MRI, controversy remains regarding the relationship between mean ADC values and lesion aggressiveness characteristics, such as histologic grade, tumor size, or axillary lymph node metastasis (37, 38). In our study, although we found that texture analysis parameters were different among the MCF-7 estradiol (+), MCF-7 estradiol (-), and MDA-MB-231 tumor groups; no significant difference was found in the mean ADC values. Therefore, we believe that texture analysis of ADC maps obtained using high-strength MRI can provide more refined information of tumor cellularity or extracellular space reflecting cellular proliferation than the mean ADC analysis of clinical MRI.

Quantification of intratumoral heterogeneity provides relevant information for making decisions during a specific treatment. The most aggressive clones within a tumor tend to survive, replicate, and metastasize during the eradication of clones sensitive to treatment (39). Serial biopsy for the metastatic lesions might be used to detect clonal evolution for targeted therapy (2). However, considering sampling bias and practical applicability issues, non-invasive monitoring methods evaluating tumor cellularity and possible epithelial mesenchymal transition by reflecting water motion changes could be a promising alternative in future research (36).

There are several limitations in this study. First, we used a 9.4T animal MR machine with a surface coil to achieve high resolution ADC map. Animal tumor models usually tend to grow more rapidly than human patient tumors, and it is known that animal tumor models show less intra- and inter-tumoral heterogeneity (31). Thus,

we cannot directly extrapolate our results to humans without further investigations. In addition, the radiofrequency field inhomogeneity of the surface coil used in our study could have exaggerated the contrast of the images, although all tumors underwent MR images by using the same surface coil. Second, we used a mono-exponential model to acquire all b-factors. Although several studies have reported that that the bi-exponential model is accurate for calculating ADC values without influence of microperfusion(40, 41), the clinical application of the bi-exponential model is still controversial(42-44). Third, MR images were obtained in different intervals between tumor implantation and MR examinations among three groups. As the growth rates of tumor groups were various, it was inevitable to obtain MR image at various intervals to minimize volumetric differences.

In conclusion, the MCF-7 tumors supplemented with estradiol showed more heterogeneous texture parameters than either the MCF-7 tumors without estradiol supplement or the MDA-MB 231 tumors, which were characterized by higher cellular proliferation and central necrosis patterns. The MDA-MB-231 tumors showed less heterogeneous texture parameters than the MCF-7 tumors due to higher vascularity and diffuse multifocal necrosis patterns. The texture analysis of the ADC maps of breast cancer xenograft models provided quantitative measurement of intratumoral heterogeneity of necrosis patterns mediated from proliferative activity and vascularity. Thus, the texture analysis of DW-MR images could be used as a non-invasive imaging method of monitoring the intratumoral heterogeneity of cellularity following therapy in breast cancer patients.

REFERENCES

1. Perou CM, Sorlie T, Eisen MB, van de Rijn M, Jeffrey SS, Rees CA et al. Molecular portraits of human breast tumours. *Nature* 2000;406:747-752
2. Bedard PL, Hansen AR, Ratain MJ, Siu LL. Tumour heterogeneity in the clinic. *Nature* 2013;501:355-364
3. Koh DM, Collins DJ. Diffusion-weighted mri in the body: Applications and challenges in oncology. *AJR Am J Roentgenol* 2007;188:1622-1635
4. Choi BB, Kim SH, Kang BJ, Lee JH, Song BJ, Jeong SH et al. Diffusion-weighted imaging and FDG PET/CT: Predicting the prognoses with apparent diffusion coefficient values and maximum standardized uptake values in patients with invasive ductal carcinoma. *World J Surg Oncol* 2012;10:126
5. Costantini M, Belli P, Distefano D, Bufi E, Matteo MD, Rinaldi P et al. Magnetic resonance imaging features in triple-negative breast cancer: Comparison with luminal and HER2-overexpressing tumors. *Clin Breast Cancer* 2012;12:331-339
6. Guo Y, Cai YQ, Cai ZL, Gao YG, An NY, Ma L et al. Differentiation of clinically benign and malignant breast lesions using diffusion-weighted imaging. *J Magn Reson Imaging* 2002;16:172-178
7. Jeh SK, Kim SH, Kim HS, Kang BJ, Jeong SH, Yim HW et al. Correlation of the apparent diffusion coefficient value and dynamic magnetic resonance imaging findings with prognostic factors in invasive ductal carcinoma. *J Magn Reson Imaging* 2011;33:102-109
8. Kamitani T, Matsuo Y, Yabuuchi H, Fujita N, Nagao M, Jinnouchi M et al.

Correlations between apparent diffusion coefficient values and prognostic factors of breast cancer. *Magn Reson Med Sci* 2013;12:193-199

9. Park SH, Moon WK, Cho N, Song IC, Chang JM, Park IA et al. Diffusion-weighted MR imaging: Pretreatment prediction of response to neoadjuvant chemotherapy in patients with breast cancer. *Radiology* 2010;257:56-63

10. Jung DC, Lee HJ, Seo JW, Park SY, Lee SJ, Lee JH et al. Diffusion-weighted imaging of a prostate cancer xenograft model seen on a 7 Tesla animal MR scanner: Comparison of ADC values and pathologic findings. *Korean J Radiol* 2012;13:82-89

11. Stephen RM, Pagel MD, Brown K, Baker AF, Meuillet EJ, Gillies RJ. Monitoring the development of xenograft triple-negative breast cancer models using diffusion-weighted magnetic resonance imaging. *Exp Biol Med (Maywood)* 2012;237:1273-1280

12. Davnall F, Yip CS, Ljungqvist G, Selmi M, Ng F, Sanghera B et al. Assessment of tumor heterogeneity: An emerging imaging tool for clinical practice? *Insights Imaging* 2012;3:573-589

13. Karahaliou A, Vassiou K, Arikidis N, Skiadopoulos S, Kanavou T, Costaridou L. Assessing heterogeneity of lesion enhancement kinetics in dynamic contrast-enhanced MRI for breast cancer diagnosis. *Br J Radiol* 2010;83:296-309

14. Haralick RM, Shanmugam K, Dinstein IH. Textural features for image classification. *IEEE Transactions on Systems, Man and Cybernetics* 1973:610-621

15. Chen W, Giger ML, Li H, Bick U, Newstead GM. Volumetric texture

analysis of breast lesions on contrast-enhanced magnetic resonance images. *Magn Reson Med* 2007;58:562-571

16. Eary JF, O'Sullivan F, O'Sullivan J, Conrad EU. Spatial heterogeneity in sarcoma 18F-FDG uptake as a predictor of patient outcome. *J Nucl Med* 2008;49:1973-1979

17. Gibbs P, Turnbull LW. Textural analysis of contrast-enhanced MR images of the breast. *Magn Reson Med* 2003;50:92-98

18. Henriksson E, Kjellen E, Wahlberg P, Ohlsson T, Wennerberg J, Brun E. 2-Deoxy-2-[18F] fluoro-D-glucose uptake and correlation to intratumoral heterogeneity. *Anticancer Res* 2007;27:2155-2159

19. Sinha S, Lucas-Quesada FA, DeBruhl ND, Sayre J, Farria D, Gorczyca DP et al. Multifeature analysis of Gd-enhanced MR images of breast lesions. *J Magn Reson Imaging* 1997;7:1016-1026

20. Tixier F, Le Rest CC, Hatt M, Albarghach N, Pradier O, Metges JP et al. Intratumor heterogeneity characterized by textural features on baseline 18F-FDG PET images predicts response to concomitant radiochemotherapy in esophageal cancer. *J Nucl Med* 2011;52:369-378

21. van Velden FH, Cheebsumon P, Yaqub M, Smit EF, Hoekstra OS, Lammertsma AA et al. Evaluation of a cumulative SUV-volume histogram method for parameterizing heterogeneous intratumoural FDG uptake in non-small cell lung cancer PET studies. *Eur J Nucl Med Mol Imaging* 2011;38:1636-1647

22. Yu H, Caldwell C, Mah K, Poon I, Balogh J, MacKenzie R et al. Automated radiation targeting in head-and-neck cancer using region-based texture

analysis of PET and CT images. *Int J Radiat Oncol Biol Phys* 2009;75:618-625

23. Stejskal E, Tanner J. Spin diffusion measurements: Spin echoes in the presence of a time-dependent field gradient. *J Chem Phys* 1965;42:288-292

24. Albregtsen F. Statistical texture measures computed from gray level coocurrence matrices. Image Processing Laboratory Department of Informatics University of Oslo, 2008, November 5

25. Huuse EM, Moestue SA, Lindholm EM, Bathen TF, Nalwoga H, Kruger K et al. In vivo MRI and histopathological assessment of tumor microenvironment in luminal-like and basal-like breast cancer xenografts. *J Magn Reson Imaging* 2012;35:1098-1107

26. Zhu Z, Edwards RJ, Boobis AR. Increased expression of histone proteins during estrogen-mediated cell proliferation. *Environ Health Perspect* 2009;117:928-934

27. Katzenellenbogen BS, Kendra KL, Norman MJ, Berthois Y. Proliferation, hormonal responsiveness, and estrogen receptor content of MCF-7 human breast cancer cells grown in the short-term and long-term absence of estrogens. *Cancer Res* 1987;47:4355-4360

28. Downey K, Riches SF, Morgan VA, Giles SL, Attygalle AD, Ind TE et al. Relationship between imaging biomarkers of stage I cervical cancer and poor-prognosis histologic features: Quantitative histogram analysis of diffusion-weighted MR images. *AJR Am J Roentgenol* 2013;200:314-320

29. Kyriazi S, Collins DJ, Messiou C, Pennert K, Davidson RL, Giles SL et al. Metastatic ovarian and primary peritoneal cancer: Assessing chemotherapy

response with diffusion-weighted MR imaging--value of histogram analysis of apparent diffusion coefficients. *Radiology* 2011;261:182-192

30. Nelson DA, Tan TT, Rabson AB, Anderson D, Degenhardt K, White E. Hypoxia and defective apoptosis drive genomic instability and tumorigenesis. *Genes Dev* 2004;18:2095-2107

31. Bokacheva L, Ackerstaff E, Lekaye HC, Zakian K, Koutcher JA. High-field small animal magnetic resonance oncology studies. *Phys Med Biol* 2013;59:R65-R127

32. Padhani AR, Liu G, Koh DM, Chenevert TL, Thoeny HC, Takahara T et al. Diffusion-weighted magnetic resonance imaging as a cancer biomarker: Consensus and recommendations. *Neoplasia* 2009;11:102-125

33. Barrett T, Gill AB, Kataoka MY, Priest AN, Joubert I, McLean MA et al. DCE and DW MRI in monitoring response to androgen deprivation therapy in patients with prostate cancer: A feasibility study. *Magn Reson Med* 2012;67:778-785

34. Vossen JA, Buijs M, Geschwind JF, Liapi E, Prieto Ventura V, Lee KH et al. Diffusion-weighted and Gd-EOB-DTPA-contrast-enhanced magnetic resonance imaging for characterization of tumor necrosis in an animal model. *J Comput Assist Tomogr* 2009;33:626-630

35. Wagner M, Maggiori L, Ronot M, Paradis V, Vilgrain V, Panis Y et al. Diffusion-weighted and T2-weighted MR imaging for colorectal liver metastases detection in a rat model at 7 T: A comparative study using histological examination as reference. *Eur Radiol* 2013;23:2156-2164

36. Chen YW, Pan HB, Tseng HH, Chu HC, Hung YT, Yen YC et al.

Differentiated epithelial- and mesenchymal-like phenotypes in subcutaneous mouse xenografts using diffusion weighted-magnetic resonance imaging. *Int J Mol Sci* 2013;14:21943-21959

37. Kim SH, Cha ES, Kim HS, Kang BJ, Choi JJ, Jung JH et al. Diffusion-weighted imaging of breast cancer: Correlation of the apparent diffusion coefficient value with prognostic factors. *J Magn Reson Imaging* 2009;30:615-620

38. Razek AA, Gaballa G, Denewer A, Nada N. Invasive ductal carcinoma: Correlation of apparent diffusion coefficient value with pathological prognostic factors. *NMR Biomed* 2010;23:619-623

39. Nowell PC. The clonal evolution of tumor cell populations. *Science* 1976;194:23-28

40. Le Bihan D, Breton E, Lallemand D, Grenier P, Cabanis E, Laval-Jeantet M. MR imaging of intravoxel incoherent motions: Application to diffusion and perfusion in neurologic disorders. *Radiology* 1986;161:401-407

41. Liu C, Liang C, Liu Z, Zhang S, Huang B. Intravoxel incoherent motion (IVIM) in evaluation of breast lesions: Comparison with conventional DWI. *Eur J Radiol* 2013

42. Doblas S, Wagner M, Leitao HS, Daire JL, Sinkus R, Vilgrain V et al. Determination of malignancy and characterization of hepatic tumor type with diffusion-weighted magnetic resonance imaging: Comparison of apparent diffusion coefficient and intravoxel incoherent motion-derived measurements. *Invest Radiol* 2013;48:722-728

43. Sigmund EE, Cho GY, Kim S, Finn M, Moccaldi M, Jensen JH et al.

Intravoxel incoherent motion imaging of tumor microenvironment in locally advanced breast cancer. *Magn Reson Med* 2011;65:1437-1447

44. Tamura T, Usui S, Murakami S, Arihiro K, Akiyama Y, Naito K et al. Biexponential signal attenuation analysis of diffusion-weighted imaging of breast. *Magn Reson Med Sci* 2010;9:195-207

Table 1. Comparison of Texture Parameters of ADC map among MCF-7 estradiol (+), MCF-7 estradiol (-), and MDA-MB-231 Groups

	MCF-7 estradiol (+) (Mean ± SD)	MCF-7 estradiol (-) (Mean ± SD)	MDA-MB-231 (Mean ± SD)	*P*-Value
First order texture				
Mean*	287 ± 70	243 ± 29	268 ± 60	0.474
First quartile*	64 ± 48	66 ± 23	89 ± 42	0.100
Second quartile* (Median)	163 ± 84	183 ± 34	241 ± 82	0.051
Third quartile*	308 ± 97	336 ± 36	388 ± 85	0.111
Standard deviation*	398 ± 61	235 ± 29	213 ± 33	**<0.001**
Maximum value*	2610 ± 290	1904 ± 275	2149 ± 440	**<0.001**
Minimum value*	0.200 ± 0.259	0.289 ± 0.285	0.333 ± 0.150	**0.025**
Skewness	2.66 ± 0.23	1.82 ± 0.29	1.23 ± 0.59	**<0.001**
Kurtosis	7.32 ± 0.93	4.69 ± 1.64	3.45 ± 2.41	**0.001**
Second order texture				
Contrast	476 ± 104	536 ± 147	288 ± 143	**0.004**
Entropy	6.42 ± 1.47	6.60 ± 1.47	6.82 ± 0.71	0.839
Homogeneity	0.287 ± 0.146	0.235 ± 0.149	0.225 ± 0.083	0.577
Uniformity	0.0560 ± 0.0953	0.0456 ± 0.0911	0.0143 ± 0.0185	0.787
Correlation†	0.437 ± 0.244	0.824 ± 0.182	2.00 ± 1.19	**<0.001**

*Unit: $x10^{-6}mm^2/sec$, †Unit: $x10^{-3}$

Table 2. Intraobserver Agreement for the Measurement of Texture Parameters

	Intraclass coefficients	95% CI*
First order texture		
Mean	0.983	0.964-0.992
Second quartile (Median)	0.974	0.943-0.988
Standard deviation	0.989	0.976-0.995
Minimum value	0.270	-0.115-0.585
Maximum value	0.885	0.763-0.946
Skewness	0.955	0.904-0.979
Kurtosis	0.935	0.864-0.970
Second order texture		
Contrast	0.989	0.976-0.995
Entropy	0.997	0.994-0.999
Homogeneity	0.999	0.998-1.000
Uniformity	0.998	0.996-0.999
Correlation(COR)	0.993	0.985-0.997

*CI : confidence interval

Table 3. Comparison of Histopathologic Features among MCF-7 estradiol (+), MCF-7 estradiol (-), and MDA-MB-231 Groups.

	MCF-7 estradiol (+) (Mean ± SD) (n=12)	MCF-7 estradiol (-) (Mean ± SD) (n=9)	MDA-MB-231 (Mean ± SD) (n=6)	*P*-Value
Proportion of necrosis (%)	23.8 ± 9.3	18.3 ± 5.0	35.8 ± 15.0	0.008
Pattern of necrosis (number, %)				
Central	10 (83)	8(89)	0 (0)	<0.001
Diffuse multifocal	2 (17)	1 (11)	6 (100)	
Ki-67 (%)				
Ki-67 mean	52.1 ± 4.6	18.9 ± 5.1	45.1 ± 5.2	<0.001
Ki-67 difference (highest-lowest)	44.3 ± 13.5	29.8 ± 10.0	26.5 ± 13.4	0.010
Microvessel density (MVD)				
MVD mean*	18 ± 9	18 ± 6	44 ± 11	<0.001
MVD difference* (highest-lowest)	22 ± 12	11 ± 6	51 ± 17	<0.001

*Unit :/HPF (high power field)

Figure 1. Box-and-whisker plot of (A) the volumes of the tumor groups and the first order texture analysis parameters, including the (B) mean, (C) median, (D) standard deviation, (E) maximum, (F) minimum, (G) skewness, and (H) kurtosis of the ADC maps for the MCF-7 estradiol (+) (dark grey boxes), MCF-7 estradiol (-) (light grey boxes), and MDA-MB-231 (white boxes) groups.

*Statistical significance with $P< 0.05$. **Statistical significance with $P< 0.01$. ***Statistical significance with $P< 0.001$. ○: Observations 1.5 interquartile ranges (IQRs) from the end of the box. ★: Observations 3 IQRs from the end of the box.

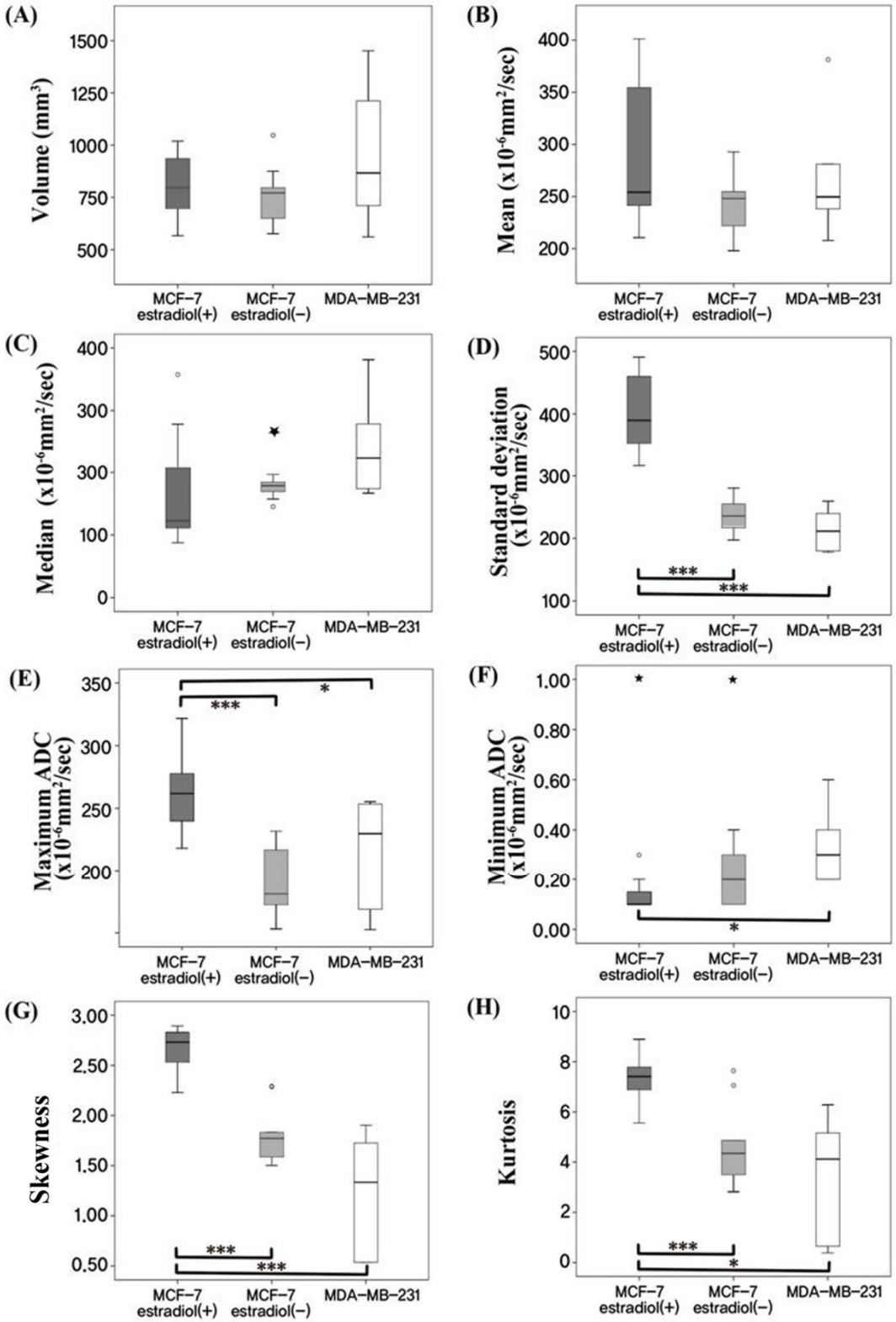
(A)
Volume (mm³)
1500
1250
1000
750
500
MCF-7 estradiol(+)
MCF-7 estradiol(−)
MDA-MB-231
(B)
Mean (x10⁻⁶mm²/sec)
400
350
300
250
200
(C)
Median (x10⁻⁶mm²/sec)
400
300
300
100
0
(D)
Standard deviation (x10⁻⁶mm²/sec)
500
400
300
200
100
***
***
(E)
Maximum ADC (x10⁻⁶mm²/sec)
350
300
250
200
***
*
(F)
Minimum ADC (x10⁻⁶mm²/sec)
1.00
0.80
0.60
0.40
0.20
0.00
*
(G)
Skewness
3.00
2.50
2.00
1.50
1.00
0.50
***
***
(H)
Kurtosis
10
8
6
4
2
0
***
*

Figure 2. Box-and-whisker plot of the second order texture analysis parameters of the tumor groups. The (A) contrast, (B) entropy, (C) homogeneity, (D) uniformity, and (E) correlation(COR) of the ADC maps for the MCF-7 estradiol (+) (dark grey boxes), MCF-7 estradiol (-) (light grey boxes), and MDA-MB-231 (white boxes) groups are shown.

*Statistical significance with $P< 0.05$. **Statistical significance with $P< 0.01$. ***Statistical significance with $P< 0.001$. ○: Observations 1.5 IQRs from the end of the box. ★: Observations 3 IQRs from the end of the box.

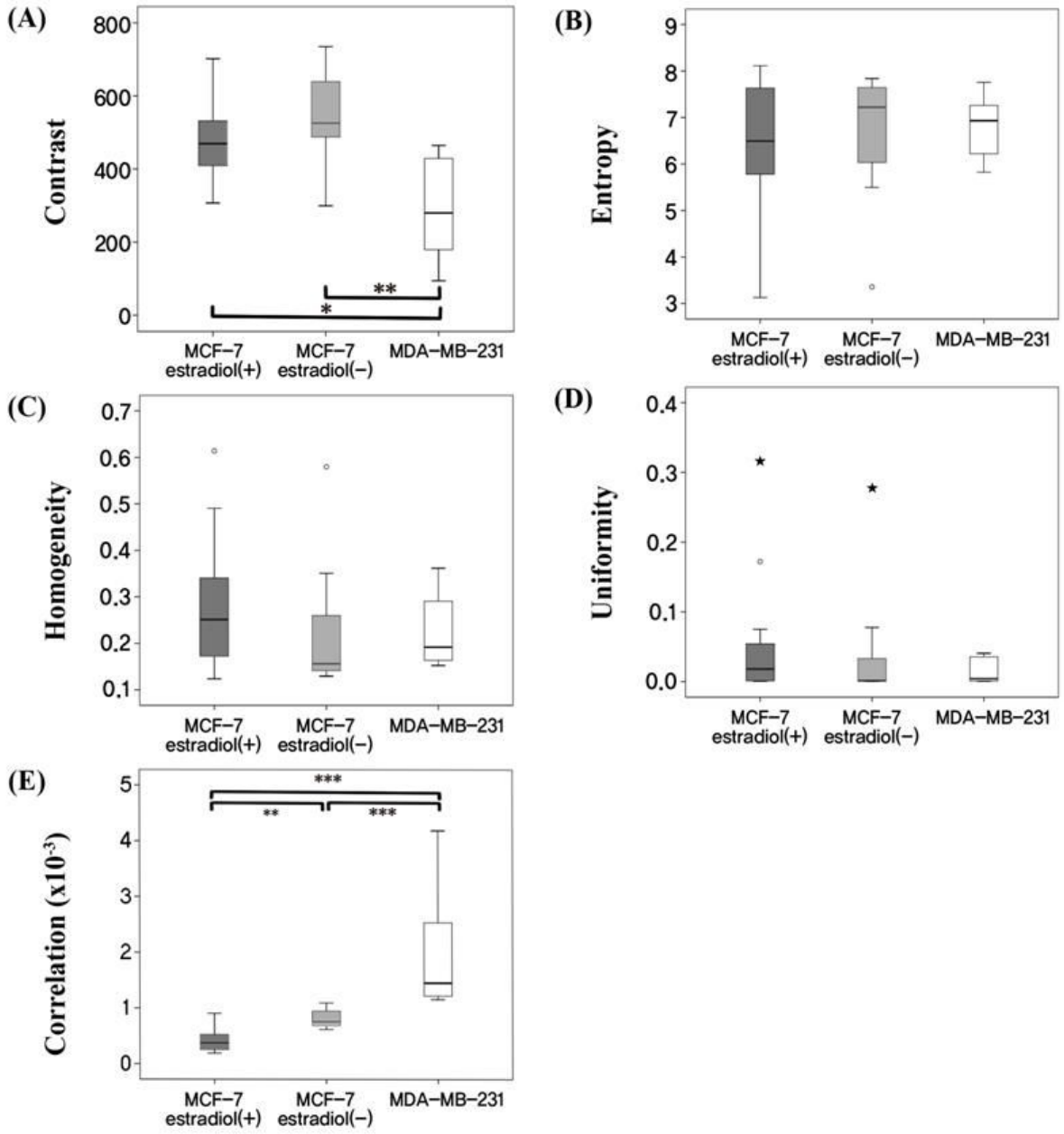
(A)
Contrast
800
600
400
200
0
**
*
MCF-7 estradiol(+)
MCF-7 estradiol(-)
MDA-MB-231
(B)
Entropy
9
8
7
6
5
4
3
MCF-7 estradiol(+)
MCF-7 estradiol(-)
MDA-MB-231
(C)
Homogeneity
0.7
0.6
0.5
0.4
0.3
0.2
0.1
MCF-7 estradiol(+)
MCF-7 estradiol(-)
MDA-MB-231
(D)
Uniformity
0.4
0.3
0.2
0.1
0.0
MCF-7 estradiol(+)
MCF-7 estradiol(-)
MDA-MB-231
(E)
Correlation (x10-3)
5
4
3
2
1
0
***
**
***
MCF-7 estradiol(+)
MCF-7 estradiol(-)
MDA-MB-231

Figure 3. Box-and-whisker plot of histopathologic features of the tumor groups. The (A) Proportion of necrosis, (B) $Ki\text{-}67_{mean}$, (C) $Ki\text{-}67_{diff}$ (highest-lowest), (D) MVD_{mean}, and (E) MVD_{diff} (highest-lowest) for the MCF-7 estradiol (+) (dark grey boxes), MCF-7 estradiol (-) (light grey boxes), and MDA-MB-231 (white boxes) groups are shown.

**Statistical significance with P< 0.05. **Statistical significance with P< 0.01. ***Statistical* significance with *P*< 0.001. ○: Observations 1.5 IQRs from the end of the box. ★: Observations 3 IQRs from the end of the box.

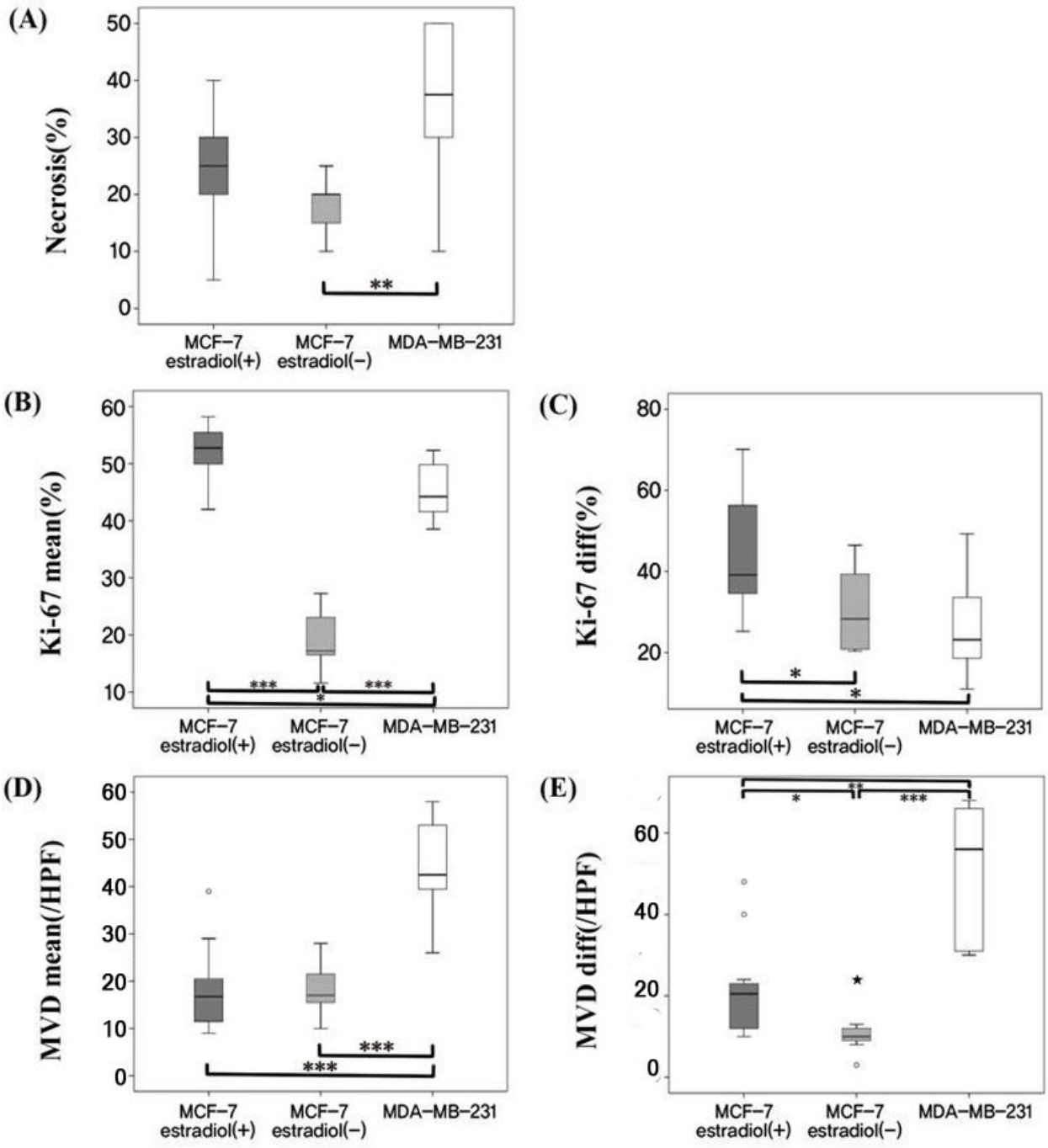
(A)
Necrosis(%)
50
40
30
20
10
0
**
MCF-7 estradiol(+)
MCF-7 estradiol(-)
MDA-MB-231
(B)
Ki-67 mean(%)
60
50
40
30
20
10
***
*
***
MCF-7 estradiol(+)
MCF-7 estradiol(-)
MDA-MB-231
(C)
Ki-67 diff(%)
80
60
40
20
*
*
MCF-7 estradiol(+)
MCF-7 estradiol(-)
MDA-MB-231
(D)
MVD mean(/HPF)
60
50
40
30
20
10
0
***
***
MCF-7 estradiol(+)
MCF-7 estradiol(-)
MDA-MB-231
(E)
MVD diff(/HPF)
60
40
20
0
*
**
***
MCF-7 estradiol(+)
MCF-7 estradiol(-)
MDA-MB-231

Figure 4. Relationship between the ADC maps and histopathologic results. Photomicrographs of the entire section show (A) central necrosis (arrow) in an MCF-7 estradiol (+) tumor and (B) diffuse multifocal necrosis (arrow) in an MDA-MB 231 tumor (H&E, ×1.25). Photomicrographs of immunohistochemical staining shows high Ki-67 expression in MCF-7 estradiol (+) tumors (C) and MDA-MB-231 tumors (D) (×200). Photomicrographs of immunohistochemical staining for CD34 show low microvessel density in MCF-7 estradiol (+) tumors (E) and high microvessel density in MDA-MB-231 tumors (F) (×200). The ADC map (G) shows higher ADC values in the central necrotic portion (arrow) and (H) spotty high ADC values (arrow) corresponding to necrosis.

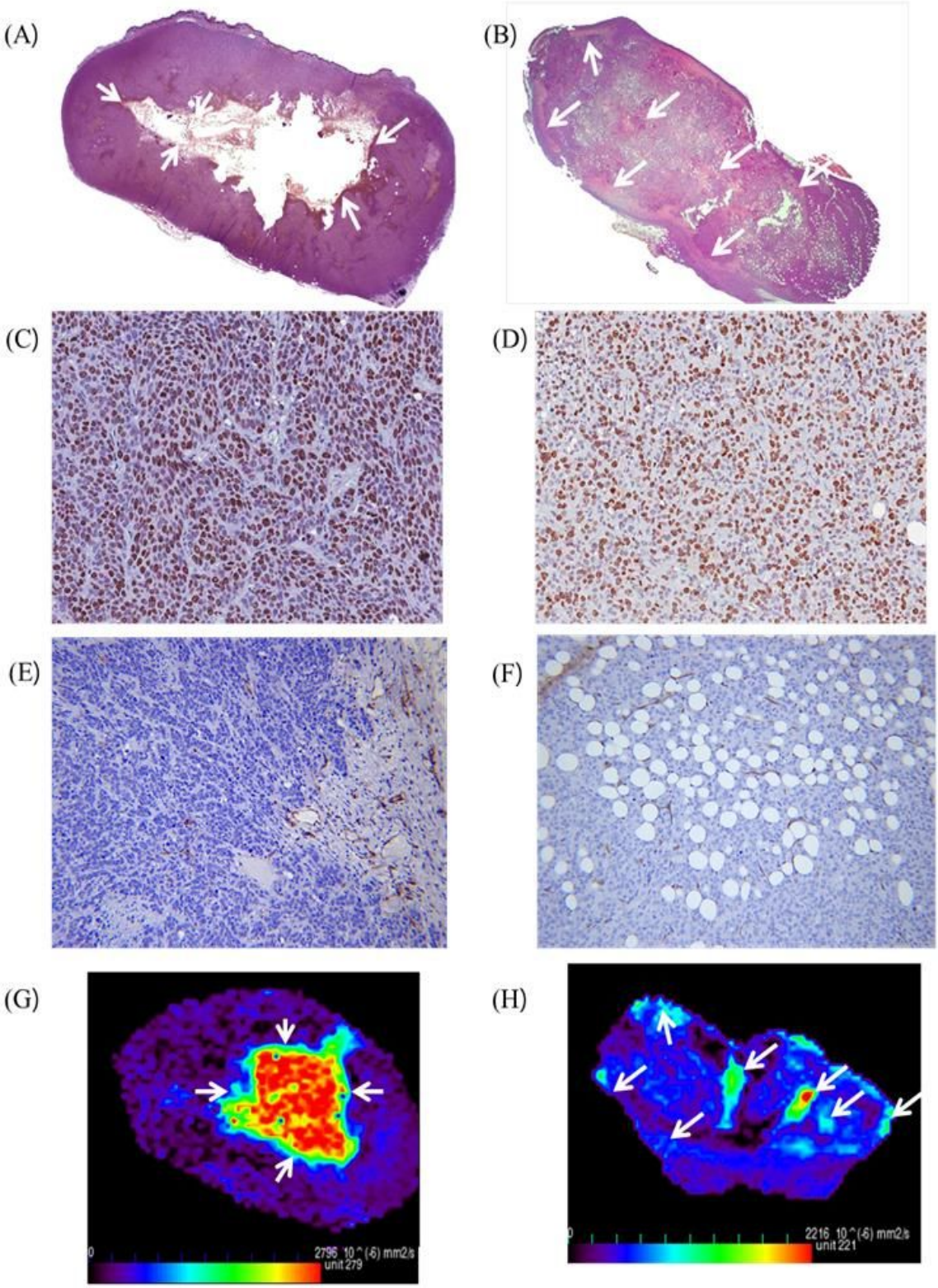
(A)
(B)
(C)
(D)
(E)
(F)
(G)
(H)
2796 10^(-6) mm2/s
unit 279
2216 10^(-6) mm2/s
unit 221

Figure 5. The relationship between the texture parameters and Ki-67 index of the tumor groups. (A) $Ki\text{-}67_{mean}$ and (B) $Ki\text{-}67_{diff}$ showed a positive correlation with the standard deviation, skewness, and kurtosis of the ADC texture parameters. However, the COR of the ADC map showed an inverse correlation with $Ki\text{-}67_{diff}$.

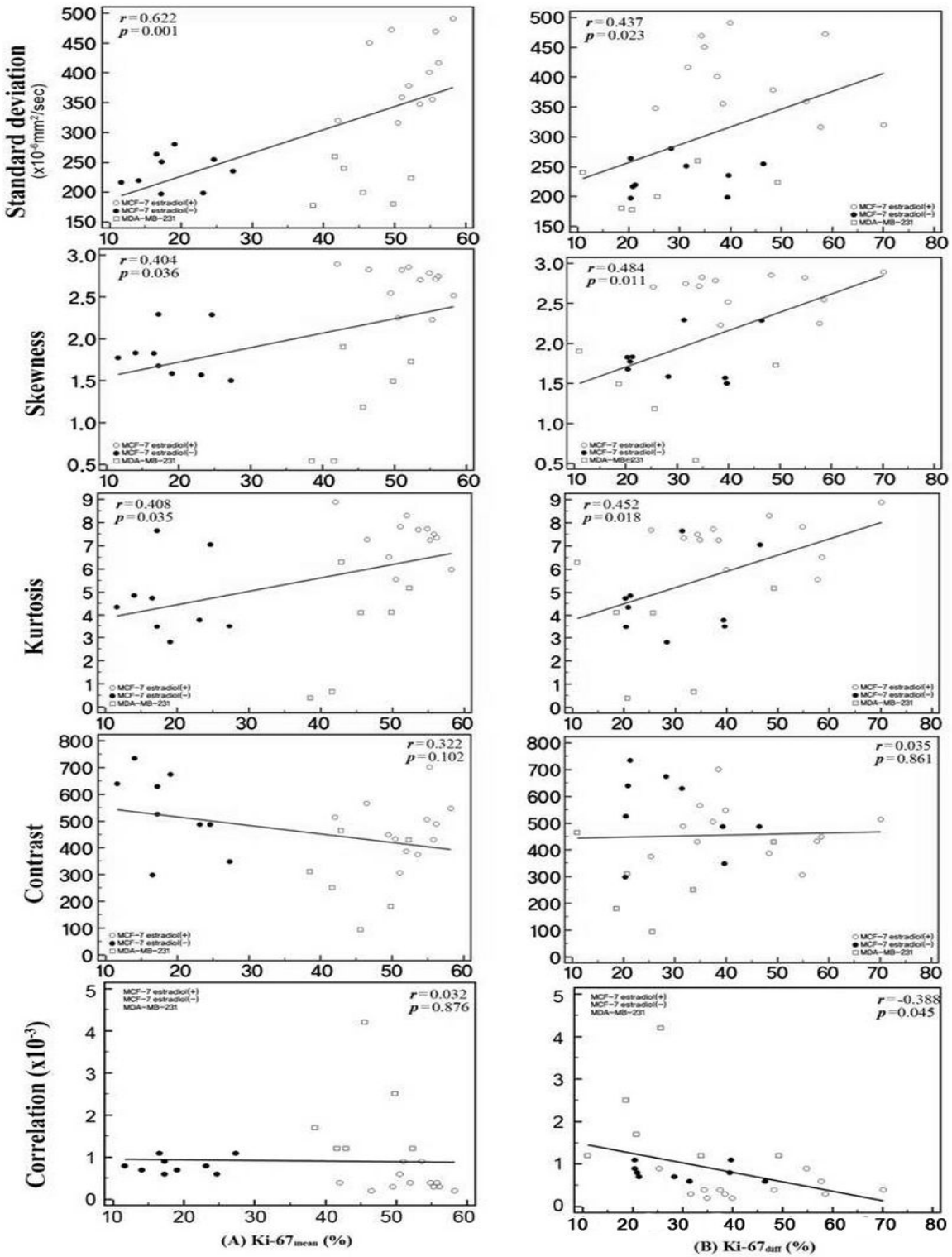
Standard deviation (x10⁻³mm²/sec)
Skewness
Kurtosis
Contrast
Correlation (x10⁻³)
r=0.622
p=0.001
r=0.437
p=0.023
r=0.404
p=0.036
r=0.484
p=0.011
r=0.408
p=0.035
r=0.452
p=0.018
r=0.322
p=0.102
r=0.035
p=0.861
r=0.032
p=0.876
r=-0.388
p=0.045
MCF-7 estradiol(+)
MCF-7 estradiol(-)
MDA-MB-231
(A) Ki-67mean (%)
(B) Ki-67diff (%)

Figure 6. The relationship between the texture parameters and MVD of the tumor groups. (A) MVD_{mean} and (B) MVD_{diff} showed an inverse correlation with skewness, kurtosis and contrast. The COR of the ADC map was correlated with MVD_{mean} and MVD_{diff}.

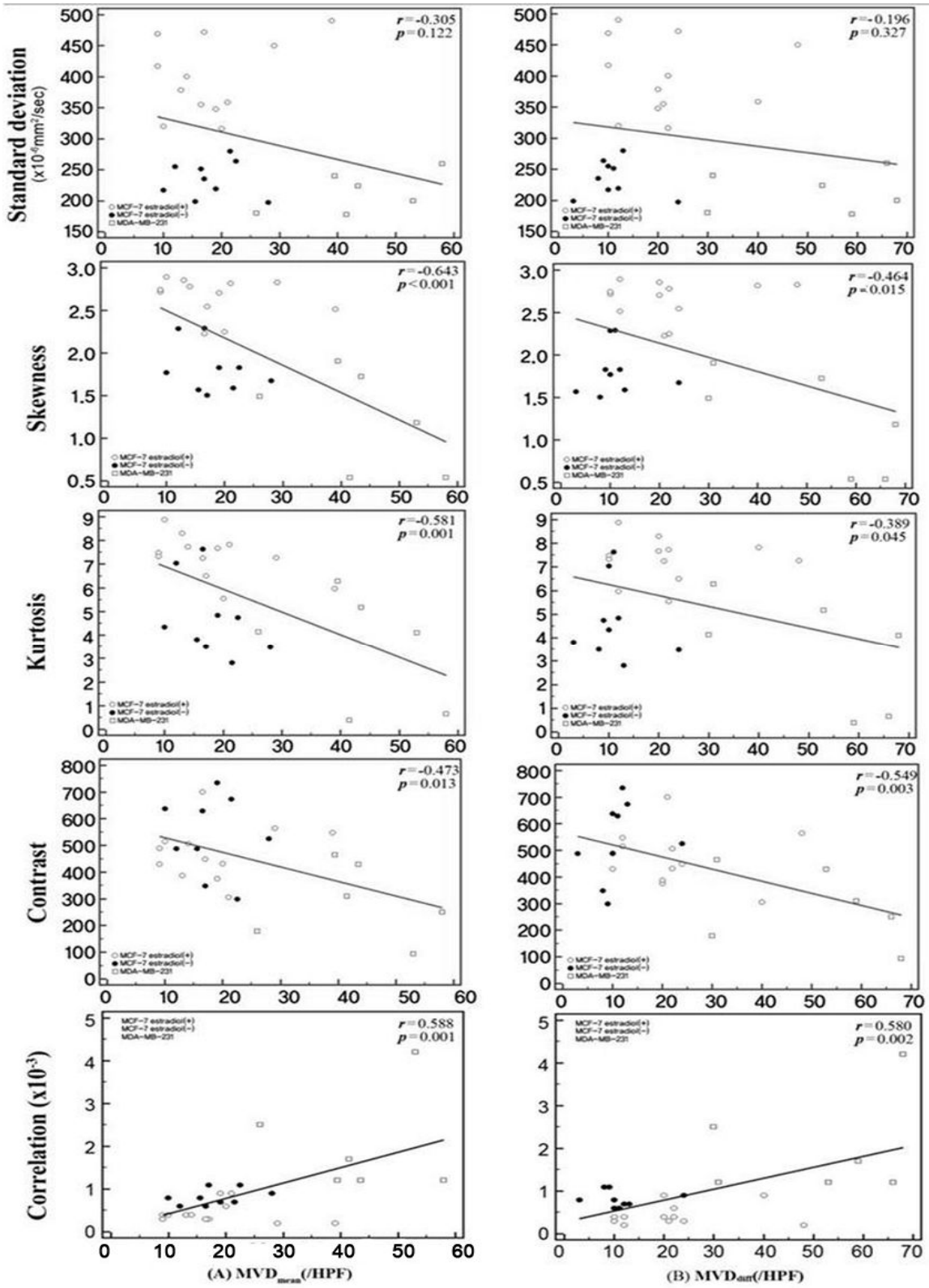
Standard deviation (x10⁻⁶mm²/sec)
r=-0.305
p=0.122
r=-0.196
p=0.327
Skewness
r=-0.643
p<0.001
r=-0.464
p=0.015
Kurtosis
r=-0.581
p=0.001
r=-0.389
p=0.045
Contrast
r=-0.473
p=0.013
r=-0.549
p=0.003
Correlation (x10⁻³)
r=0.588
p=0.001
r=0.580
p=0.002
MCF-7 estradiol(+)
MCF-7 estradiol(-)
MDA-MB-231
(A) MVD_mean(/HPF)
(B) MVD_sum(/HPF)

Figure 7. Three simulations of different correlations. First-order texture parameters are identical for the three cases, mean= 1.5 and standard deviation = 0.5 in all matrices. However, the second-order texture parameters derived from the grey level co-occurrence matrix (GLCM) varied. (A) The most heterogeneous mosaic pattern matrix shows the lowest correlation value, -0.09. (B) The intermediate pattern shows the correlation is 0.49. (C) The pattern with largest area of same value shows the highest correlation, 0.75.

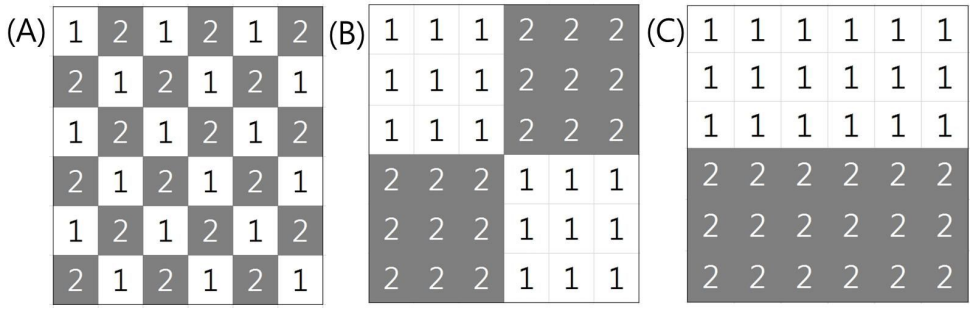

국문초록

목적: MCF-7과 MDA-MB-231 인간 유방암 세포주 이종이식 동물 모델에서 현성확산계수(ADC)의 텍스쳐 파라미터들과 병리학적 특성과의 관련성을 평가하고자 한다.

방법: 동물실험윤리위원회의 승인 후, SCID mouse를 이용해 MCF-7 estradiol (+)와 MCF-7 estradiol (-), MDA-MB-231 유방암 세포주 이종이식 동물 모델을 만들었다. 9.4T MR에서 확산강조영상을 획득하였다. ADC 맵에서 일차 텍스쳐 분석과 Grey level co-occurrence matrix (GLCM)을 이용한 이차 텍스트 분석을 시행하였다. 세 군에서 얻은 영상파라미터와 병리학적 특징을 변량분석을 통해 비교하였다. 관찰자 내 일치도는 급내상관계수로 평가하였다. 영상파라미터와, 종양괴사정도와 형태, 세포 증식 정도, 미세혈관밀도(MVD) 등의 병리학적인 특징을 피어슨 상관분석을 통해 비교하였다. 결과는 estradiol을 투여한 MCF-7 모델의 종양 12개, estradiol을 투여하지 않은 MCF-7 모델의 종양 9개, MDA-MB-231 모델의 종양 6개를 분석하였다.

결과: 일차 텍스쳐 분석에서, MCF-7 estradiol (+) 군은 표준편차와 최대값, 첨도, 왜도가 MCF-7 estradiol (-)와 MDA-MB-231군에 비해 높았다. GLCM을 이용한 이차 텍스쳐 분석에서 Contrast는 estradiol 여부와 상관없이 MCF-7군이 MDA-MB-231군보다 높았다. Correlation은 estradiol 여부와 상관없이 MCF-7군이 MDA-MB-231군보다 낮았다. 2회의 텍스쳐 분석측정값 사이의 급내상관계수는 최소값을 제외한 다른 값에서 모두 0.85를 초과하여 높은 일치도를

보였다. 병리적 특징분석에서 세포 증식 정도를 나타내는 파라미터인 $Ki-67_{mean}$은 MCF-7 estradiol (+) 군이 MDA-MB-231, MCF-7 estradiol(-)보다 높았다. MVD_{mean}과 MVD_{diff}의 경우 MDA-MB-231 군이 제일 높았고 MCF-7 군이 낮았다. MDA-MB-231 군은 여러 개의 분산된 형태의 괴사를 보였고 MCF-7 군은 중심성 괴사의 모습을 주로 보였다. $Ki-67_{mean}$, $Ki-67_{diff}$와 ADC 맵에서의 표준편차 (r = 0.622, r = 0.437), 왜도 (r = 0.404, r = 0.484), 첨도 (r = 0.408, r = 0.452)는 양의 상관관계가 있었다. $Ki-67_{diff}$ 과 Correlation은 음의 상관관계가 있었다(r = −0.388, P = 0.045). MVD_{mean}, MVD_{diff}와 ADC 맵에서의 왜도 (r = −0.643, r =−0.464), 첨도 (r = −0.581, r = −0.389), Contrast (r = −0.473, r = −0.549)는 음의 상관관계가 있었다. MVD_{mean}, MVD_{diff}와 correlation은 양의 상관관계가 있었다(r = 0.588, P = 0.001; r = 0.580, P = 0.002). Contrast는 괴사 정도와 음의 상관관계가 있었다(r = −0.438, P = 0.022).

결론: ADC 맵의 텍스쳐 분석은 MCF-7 과 MDA-MB-231 인간 유방암 세포주 이종이식 종양 모델에서 괴사 패턴의 공간적 이질성과 세포 증식정도, 혈관성을 밝힐 수 있을 것으로 생각된다.

주요어: 동물; 유방암; 확산강조영상; 컴퓨터이용영상해석

학번: 2012-30515